Significance of aerosol radiative effect in energy balance control on global precipitation change

ATMOSPHERIC SCIENCE LETTERS
Atmos. Sci. Let. **18**: 389–395 (2017)
Published online in Wiley Online Library
(wileyonlinelibrary.com) **DOI:** 10.1002/asl.780

RMetS
Royal Meteorological Society

Significance of aerosol radiative effect in energy balance control on global precipitation change

Kentaroh Suzuki,[1]* Graeme L. Stephens[2,3] and Jean-Christophe Golaz[4]

[1]*Atmosphere and Ocean Research Institute, University of Tokyo, Kashiwa, Japan*
[2]*Jet Propulsion Laboratory, California Institute of Technology, Pasadena, USA*
[3]*Department of Meteorology, University of Reading, Reading, UK*
[4]*Lawrence Livermore National Laboratory, Livermore, CA, USA*

**Correspondence to:*
K. Suzuki, Atmosphere and Ocean Research Institute, University of Tokyo, 5-1-5 Kashiwanoha, Kashiwa, Chiba 277-8568, Japan.
E-mail: ksuzuki@aori.u-tokyo.ac.jp

Received: 26 April 2017
Revised: 21 July 2017
Accepted: 24 August 2017

Abstract

Historical changes of global precipitation in the 20th century simulated by a climate model are investigated. The results simulated with alternate configurations of cloud microphysics are analyzed in the context of energy balance controls on global precipitation, where the latent heat changes associated with the precipitation change is nearly balanced with changes to atmospheric radiative cooling. The atmospheric radiative cooling is dominated by its clear-sky component, which is found to correlate with changes to both column water vapor and aerosol optical depth (AOD). The water vapor-dependent component of the clear-sky radiative cooling is then found to scale with global temperature change through the Clausius–Clapeyron relationship. This component results in a tendency of global precipitation increase with increasing temperature at a rate of approximately 2%K^{-1}. Another component of the clear-sky radiative cooling, which is well correlated with changes to AOD, is also found to vary in magnitude among different scenarios with alternate configurations of cloud microphysics that controls the precipitation efficiency, a major factor influencing the aerosol scavenging process that can lead to different aerosol loadings. These results propose how different characteristics of cloud microphysics can cause different aerosol loadings that in turn perturb global energy balance to significantly change global precipitation. This implies a possible coupling of aerosol–cloud interaction with aerosol–radiation interaction in the context of global energy balance.

Keywords: **global energy balance; aerosol radiative effect; cloud microphysics; hydrologic sensitivity**

1. Introduction

Climatic change of global-mean precipitation has yet to be fully understood as illustrated by a substantial diversity in the hydrologic sensitivity, defined as the global-mean precipitation increase per increase in global-mean surface air temperature, among state-of-the-art global climate models (Pendergrass and Hartmann, 2012, 2014) particularly in the context of historical climate change (Fläschner *et al.,* 2016; Salzmann, 2016).

It is well understood that global-mean precipitation change is constrained by energy balance controls where the change to the latent heat released by precipitation is nearly balanced with change to atmospheric radiative cooling (e.g. Allen and Ingram, 2002). Such energy balance controls explain why the precipitation increase per degree in the temperature rise (~2%K^{-1}) in warmed climate induced by increased carbon dioxide (CO_2) does not keep pace with the corresponding increase in water vapor amount that primarily follows the Clausius–Clapeyron relationship (~6–7%K^{-1}) (Stephens and Ellis, 2008; Stephens and Hu, 2010). Full understanding of mechanisms determining the hydrologic sensitivity and its inter-model spread, however, has not yet been provided.

Factors influencing a global energy balance component can modify the hydrologic sensitivity as argued by Stephens and Hu (2010), who summarized the factors and their respective uncertainties to point out aerosol effects and cloud feedbacks as among the most uncertain factors. Absorbing aerosols heat the atmosphere and thus decrease the radiative cooling, which is then compensated for by a decrease in precipitation. Aerosols have also been pointed out by Pendergrass and Hartmann (2012) as a main contributor to the inter-model spread of hydrologic sensitivity. Cloud radiative feedback, whose sign is *a priori* unknown, is another source of uncertainty. When a climate model is driven by a strong positive cloud feedback on atmospheric radiative cooling, the hydrologic sensitivity becomes significantly larger (Mauritsen and Stevens, 2015) than represented by model-ensemble mean exerting slightly negative cloud feedback (Pendergrass and Hartmann, 2014). The inter-model spread in the hydrologic sensitivity has been traced to the spread of shortwave (SW) clear-sky radiative cooling (Pendergrass and

Table 1. Values of parameters α ($Wm^{-2}\,\%^{-1}$), β (Wm^{-2}), κ ($\%\,K^{-1}$) and λ ($Wm^{-2}\,K^{-1}$) as determined by least-square fit of Equations (3), (5) and (6) to the model output. The numbers in parenthesis show corresponding uncertainty range returned by the fitting routine.

	α_{SW}	α_{LW}	α	κ	β_{SW}	β_{LW}	β	λ_{SW}	λ_{LW}	λ
CM3w	−0.16 (0.009)	+0.41 (0.008)	+0.25 (0.004)	6.08 (0.04668)	14.46 (1.817)	25.45 (1.59)	39.91 (0.81)	−0.16 (0.0045)	0.22 (0.0083)	0.06 (0.005)
CM3	−0.156 (0.008)	+0.41 (0.007)	+0.253 (0.004)	6.45992 (0.09551)	20.16 (0.83)	20.43 (0.67)	40.5954 (0.4169)	−0.217 (0.0066)	0.246 (0.014)	0.029 (0.0138)
CM3c	−0.147 (0.009)	+0.43 (0.006)	+0.282 (0.004)	5.40788 (0.1379)	22.62 (0.635)	21.44 (0.47)	44.0643 (0.3036)	−0.19 (0.0085)	0.321 (0.018)	0.130 (0.0154)
Mean	−0.15 (0.009)	+0.42 (0.007)	+0.26 (0.004)	6.0 (0.09)	19.1 (1.094)	22.4 (0.91)	41.5 (0.51)	−0.19 (0.0065)	0.26 (0.0134)	0.073 (0.0114)

Hartmann, 2014), which is further broken down to different factors such as aerosol absorption (Pendergrass and Hartmann, 2012) and water vapor heating in the SW (DeAngelis *et al.,* 2015).

These uncertainties of factors influencing the atmospheric radiative cooling also impose substantial uncertainties on historical changes of the global precipitation simulated by climate models. Due to a lack of reliable, long-term precipitation measurements covering a whole globe, simulated historical changes of the global-mean precipitation are much less constrained with observations compared to those of the global-mean surface air temperature. Another uncertainty arises from ambiguous definition of the hydrologic sensitivity, which mixes up the rapid adjustment and slow response of the energy balance perturbation (Fläschner *et al.,* 2016).

Although the previous studies have shed a light on fundamental mechanisms determining the hydrologic sensitivity and possible causes for its inter-model spread, many of them are based on analysis of climate model simulations with carbon dioxide (CO_2) forcing only, which excludes impact of the aerosol radiative effect on precipitation. Key exceptions are some studies that examine experiments with individual forcing agent perturbed (Andrews *et al.,* 2010; Ming *et al.,* 2010; Samset *et al.,* 2016). These studies demonstrate how differing effects of various forcing agents on atmospheric radiation lead to distinctly different responses of global precipitation. The forcing drivers that directly affect the atmospheric radiative heating (e.g. black carbon) tend to cause a significant inter-model spread of the hydrologic sensitivity through the uncertainty of "rapid adjustment" to the forcings in climate models.

To put the results from the previous studies in the context of historical climate change, this study explores the climatic change of global precipitation manifested in 'full-forcing' historical climate simulations obtained from a coupled climate model to assess joint effect of aerosol, water vapor and cloud feedback on global precipitation. A particular focus is placed on effect of alternate configurations of cloud microphysical assumptions on global precipitation change. The differing microphysical assumptions have been found to induce significantly different magnitudes of the aerosol indirect forcing (Golaz *et al.,* 2011) and thus cause severely different historical trends of global temperature change (Golaz *et al.,* 2013). The present study is also intended to complement these studies through investigating historical change of global precipitation and its sensitivity to the cloud microphysical assumptions that influence the aerosol direct effect, as well as the indirect effect, through modulating aerosol loadings via changing the scavenging efficiency. We show that the transient climatic change of global precipitation is decomposed into a temperature-mediated component and a component closely correlated with changes of AOD. The latter is then found to significantly vary in magnitude among scenarios with different configurations of cloud microphysics, illustrating a significance of aerosol radiative effect and its modulation by cloud microphysics on historical change of global precipitation.

2. Model data

This study uses the simulation data obtained from 20th century historical climate change experiments (Golaz *et al.,* 2013) with the Geophysical Fluid Dynamics Laboratory (GFDL) Coupled Model version 3 (CM3) (Donner *et al.,* 2011). The simulations are performed with three alternate configurations of an uncertain cloud parameter, that is, the threshold particle size for warm rain to form. The scenarios with the three configurations based on the threshold particle size of 6.0, 8.2 and 10.6 μm are denoted by CM3w, CM3 and CM3c, respectively. These scenarios are based on identical forcing and emissions described by Donner *et al.* (2011) with re-tuning of a few cloud parameters listed in Table 1 of Golaz *et al.* (2013). The alternate configurations induce differing magnitudes of the aerosol indirect forcing manifested in reflected SW radiation (Figure S1(c), Supporting information), leading to severely different historical trends of global-mean temperature change (Golaz *et al.,* 2013). This study analyzes annual and global averages of the model data for the period from 1860 to 2005 after applying 5-year running mean following the analysis of Golaz *et al.* (2013). Note that our analysis has not removed the linear trend in the control simulation contrary to Golaz *et al.* (2013).

Figures 1(a) and (b) show the historical trends of global-mean surface air temperature and surface precipitation in the form of their anomalies relative to the averages over 1881–1920 for the three scenarios. These plots indicate that the global precipitation and temperature tend to vary in phase generally. This correspondence is also found in the scatter plot of the fractional change in global precipitation as a function of global temperature change (Figure 1(c)). Figure 1(c)

Table 2. Values of parameters α_{abs} ($Wm^{-2}\%^{-1}$) and β_{abs} (Wm^{-2}) for the case of employing the absorptive aerosol optical depth (AAOD) as Equation (4).

	$\alpha_{abs,sw}$	$\alpha_{abs,lw}$	α_{abs}	$\beta_{abs,sw}$	$\beta_{abs,lw}$	β_{abs}
CM3w	−0.187 (0.01)	0.421 (0.006)	0.234 (0.007)	164.252 (36.69)	509.593 (21.52)	673.801 (25.05)
CM3	−0.163 (0.011)	0.421 (0.005)	0.258 (0.008)	363.838 (21.18)	419.083 (9.291)	782.92 (16.36)
CM3c	−0.137 (0.011)	0.438 (0.004)	0.300 (0.009)	436.506 (16.48)	438.277 (6.461)	874.794 (12.48)
Mean	−0.162 (0.01)	0.427 (0.005)	0.265 (0.008)	321.532 (24.78)	455.651 (12.424)	777.183 (17.96)

shows that the precipitation tends to increase as the temperature warms approximately at a rate of $\sim 2\%K^{-1}$. However, there also exists a significant negative offset that deviates the tendency of precipitation change from the $\sim 2\%K^{-1}$ line. The negative offset is shown to be closely correlated with changes to global-mean AOD in the following analysis. Factors that can modify the slope ($\sim 2\%K^{-1}$) are also discussed below to demonstrate that the cloud feedback has a small net effect on global precipitation change in this particular climate model. The slope is then shown to be primarily determined by longwave (LW) clear-sky water vapor cooling, which owes its existence to the strong correlation of water vapor amount with global-mean temperature (Figure 1(d)) regulated by the Clausius–Clapeyron relationship as proposed by previous studies (Stephens and Ellis, 2008; Stephens and Hu, 2010).

3. Energy budget analysis

3.1. Radiative-convective equilibrium

The global-mean precipitation change is constrained by energy balance. The global energy budget states that the climatic change in latent heating associated with global-mean precipitation change ($L\Delta P$) is balanced by changes to the sensible heat flux (ΔS) and to the atmospheric radiative cooling (ΔR_{atm}) as (e.g. Allen and Ingram, 2002; Stephens and Ellis, 2008; Pendergrass and Hartmann, 2014).

$$L\Delta P + \Delta S = \Delta R_{atm}. \tag{1}$$

Assuming that ΔS is relatively small compared to other two terms, this results in the so-called radiative–convective equilibrium:

$$L\Delta P \sim \Delta R_{atm} = \Delta R_{atm,clr} - \Delta C, \tag{2}$$

where the radiative cooling (ΔR_{atm}) is further decomposed into the clear-sky component ($\Delta R_{atm,clr}$) and the cloud radiative effect (ΔC). Figure 2 shows how the balance relationships (1) and (2) applies to the historical model output of ΔP (Figure 1(b)) and ΔR_{atm} (Figure S1(d)) when Δ is defined as anomaly relative to the average over 1881–1920. Comparisons between Figures 2(a) and (b) highlight contributions from the sensible heat that becomes larger in later years of simulation. Although this change is substantial, the overall contribution of ΔS is approximately within $\sim 0.5\ Wm^{-2}$.

3.2. Clear-sky radiative cooling

Climatic changes to the clear-sky radiative cooling ($\Delta R_{atm,clr}$) is primarily determined by changes to column water vapor amount ($\Delta W/W$) and AOD ($\Delta\tau_a$) as

$$\Delta R_{atm,clr} \approx \alpha \frac{\Delta W}{W} - \beta \Delta \tau_a, \tag{3}$$

where α and β are parameters that are inherently determined by radiative process parameterizations and aerosol optical characteristics, respectively. Note that the first term in Equation (3) is an approximation to the fundamental power-law dependency of $R_{atm,clr}$ on W regulated by the radiation physics, and therefore α is a somewhat empirical parameter compared to the fundamental exponent parameter in the power-law relationship (Stephens and Hu, 2010). The second term in Equation (3) represents the aerosol heating effect with its light absorption. This could be better represented with absorptive component of AOD (AAOD), τ_{abs}, used in place of τ_a as

$$\Delta R_{atm,clr} \approx \alpha_{abs} \frac{\Delta W}{W} - \beta_{abs} \Delta \tau_{abs} \tag{4}$$

where α_{abs} and β_{abs} are the coefficients updated to fit AAOD instead of AOD.

To investigate the relationship (3) and (4), the shortwave and longwave components of $\Delta R_{atm,clr}$ are first plotted against historical change of $\Delta W/W$ (Figure S1(a)) in Figure 3. The figure shows a dominant effect of water vapor change on atmospheric radiative cooling, which is represented as the first term of (3) and (4). At the same time, however, the plots have significant scatters that are not correlated with the water vapor change. This scattered variation turns out to be closely correlated with the changes to AOD and AAOD as discussed below.

To support this point, the parameters α and β in Equation (3) (or α_{abs} and β_{abs} in Equation (4)) are determined by multi-variant least-square fit to the model output of $\Delta R_{atm,clr}$, ΔW, $\Delta\tau_a$ (Figure S1(b)) and $\Delta\tau_{abs.}$ The parameter values thus determined are listed in Table 1 and 2. Based on these parameter values, the component in $\Delta R_{atm,clr}$ that cannot be explained by ΔW/W is plotted against $\Delta\tau_a$ or $\Delta\tau_{abs}$ in Figure 4. Figure 4 illustrates that the component that does not scale with water vapor change is well correlated with changes to both AOD and AAOD, demonstrating that the least-square fitting works well to the model output. Although AAOD is more directly relevant to light absorption effect of

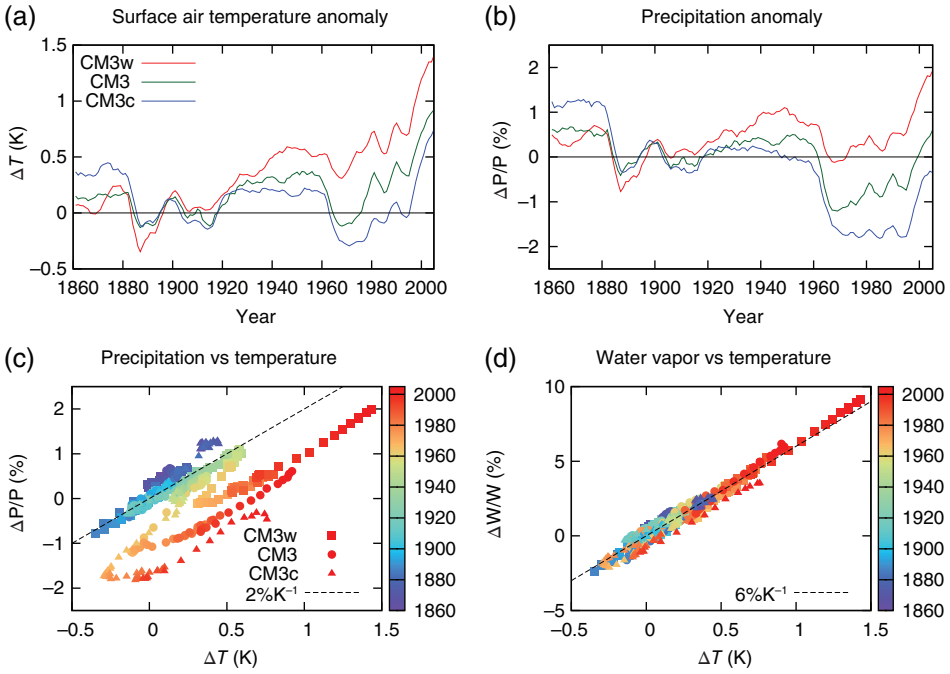

Figure 1. (a and b) Time series of global-mean surface air temperature anomaly in K (a) and precipitation anomaly in % (b). (c and d) Scatter plot of the fractional change of global precipitation (c) and column water vapor (d) as a function of global-mean temperature change. Also shown by black lines are the 2% K^{-1} (c) and 6% K^{-1} (d) slopes. In panels (c) and (d), simulation years from 1860 to 2005 are shown in different colors. The annual- and global-mean values after applying the 5-year running mean are shown.

aerosols, we employ AOD in the following analysis given its better availability as a model diagnostic.

The water vapor change $\Delta W/W$ is also closely related with the temperature change through the Clausius–Clapeyron relationship as

$$\frac{\Delta W}{W} \sim \kappa \Delta T, \tag{5}$$

where κ is approximately $6\%K^{-1}$ as shown in Figure 1(d).

3.3. Cloud radiative effect

The cloud radiative effect ΔC, another component that determines the atmospheric radiative cooling as shown in Equation (2), can also be related to the global temperature change ΔT as.

$$\Delta C \sim \lambda \Delta T, \tag{6}$$

where λ represents the sign and magnitude of the temperature-mediated change to atmospheric cloud radiative effect, which acts to change the global precipitation. The least-square fit is again applied to the model output of ΔC and ΔT (Figure S2) to determine λ for SW and LW separately (Table 1). It should also be noted that Equation (6) ignores the changes to cloud radiative effects due to aerosol impacts on clouds. Although it is not *a priori* clear whether they can be ignored particularly given uncertainties of indirect and semi-direct effects of aerosols, ΔC (Figure S2) is smaller than $\Delta R_{\mathrm{atm,clr}}$ (Figure 3) by an order of magnitude and well scales with ΔT in this model. This may arguably allow us to assume the relationship (6) in the present analysis.

The results included in Table 1 show that in this model the cloud feedbacks are positive in SW and negative in LW, resulting in a net small negative feedback on global precipitation. As will be discussed in subsection below, the magnitudes of cloud feedback components in either SW or LW are significantly smaller compared to the water vapor effects on clear-sky radiative cooling in this model similar to other models (e.g. Stephens and Ellis, 2008; Pendergrass and Hartmann, 2014). The SW and LW cloud feedbacks also have opposite signs to each other, which further result in a smaller net negative cloud feedback on global precipitation. It should be noted, however, that the magnitude and sign of cloud feedback is still highly unknown and there is no *a priori* reason for assuming that it is either positive or negative (Stephens and Hu, 2010; Mauritsen and Stevens, 2015).

3.4. Total change of global precipitation

Substituting Equations (3), (5) and (6) into (2), we obtain.

$$L\Delta P \sim (\alpha\kappa - \lambda)\,\Delta T - \beta \Delta \tau_a. \tag{7}$$

This means that the global precipitation change is comprised of two parts: a component scaling with global temperature change ΔT and a component that is correlated with changes to AOD $\Delta\tau_a$. The correlation between ΔT and $\Delta\tau_a$ are 0.8494 (CM3w), 0.5942 (CM3) and 0.1447 (CM3c), which suggests that the

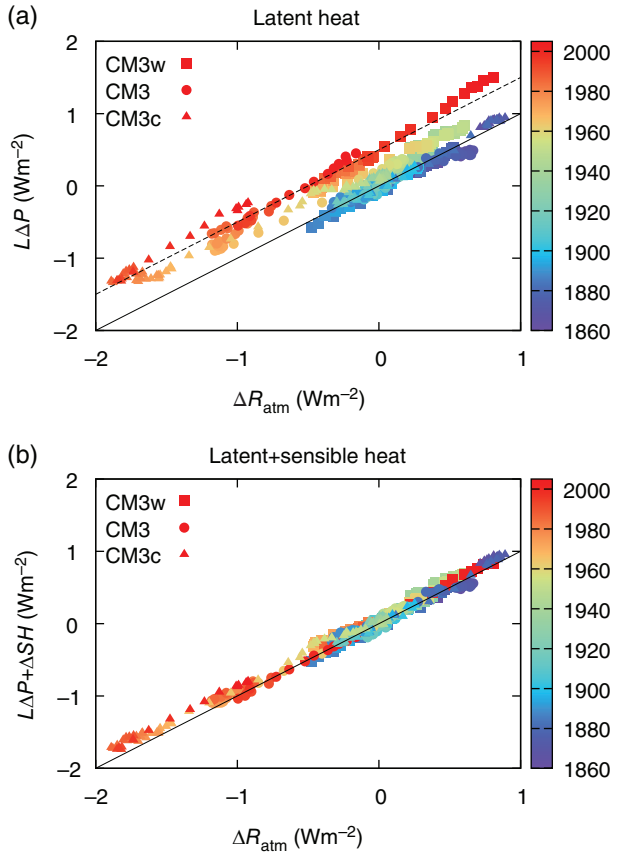

Figure 2. Scatter plot of (a) the latent heat change associated with the global precipitation change and (b) the latent plus sensible heat change, both as a function of changes to atmospheric radiative cooling rate. Different colors in each panel show simulation years from 1860 to 2005. Each point represents global- and annual-mean value after applying the 5-year running mean.

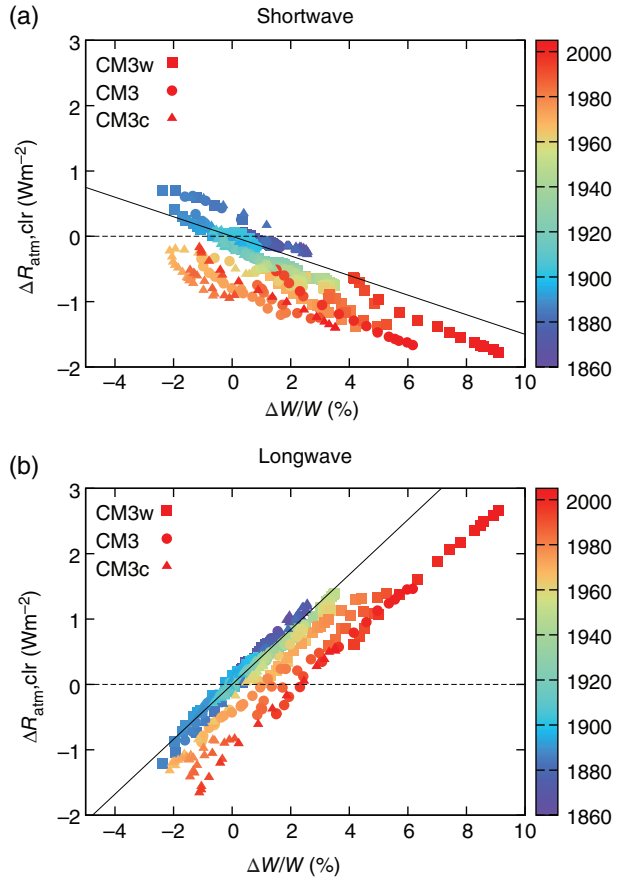

Figure 3. Scatter plot of changes to clear-sky atmospheric radiative cooling as a function of fractional changes to column water vapor amount for (a) shortwave and (b) longwave components. The solid lines represent the relationship $\Delta R_{atm,clr} = \alpha \Delta W/W$ with $\alpha_{SW} = -0.15\,\mathrm{Wm^{-2}\%^{-1}}$ and $\alpha_{LW} = +0.42\,\mathrm{Wm^{-2}\%^{-1}}$ as determined to be inter-scenario mean values of the coefficients in Table 1.

overall correlation across the three scenarios is basically low.

According to the parameter values determined above (Table 1), $\alpha\kappa \sim 1.56\,\mathrm{Wm^{-2}\,K^{-1}}$ and $\lambda \sim 0.07\,\mathrm{Wm^{-2}\,K^{-1}}$, resulting in the slope value of $\alpha\kappa - \lambda \sim 1.49\,\mathrm{Wm^{-2}\,K^{-1}}$, which roughly corresponds to $\sim 1.8\%\mathrm{K^{-1}}$. This means that the rate of increase in global precipitation with increasing global temperature is primarily determined by water vapor radiative cooling with a slight negative cloud feedback in this model.

The precipitation change is also substantially influenced by the aerosol change as represented by the second term in Equation (7). The parameter β represents the so-called radiative forcing efficiency by total aerosols (for atmospheric layer in this case), that is, the forcing per unit AOD change. This parameter, fundamental to the aerosol radiative effect, depends on various uncertain factors including aerosol optical properties, vertical aerosol profiles and the surface albedo. Such uncertainty of β is combined with uncertainty of $\Delta\tau_a$ to cause a significant uncertainty for magnitude of the aerosol radiative effect $(-\beta\Delta\tau_a)$. This makes the prediction of global precipitation change more uncertain than is the case when only the temperature-mediated component [i.e. the first term in Equation (7)] is accounted for as is the case in analysis of simulations with only CO_2 perturbed. We interpret that the uncertainty of the aerosol contribution to the atmospheric energy balance, illustrated by the second term in Equation (7), could be a major source of the inter-model spread of the hydrologic sensitivity as proposed by Pendergrass and Hartmann (2012). Our finding provides a quantitative estimate of the aerosol contribution to energy balance controls on global precipitation in the context of historical climate change simulated in a particular climate model.

The total precipitation change obtained from the historical simulations is summarized in Figure 5 as a function of the global-mean temperature change in the form that also depicts the influences from aerosol radiative effects. The theoretical relationships given by (7) are also superimposed to illustrate how the global precipitation varies as a function of both changes to global-mean temperature and AOD. Figure 5 also summarizes the historical model output colored according to the AOD anomaly to demonstrate how the precipitation anomaly deviates from the temperature-mediated relationship as the AOD anomaly increases. The deviation is also found to be larger in scenarios with larger

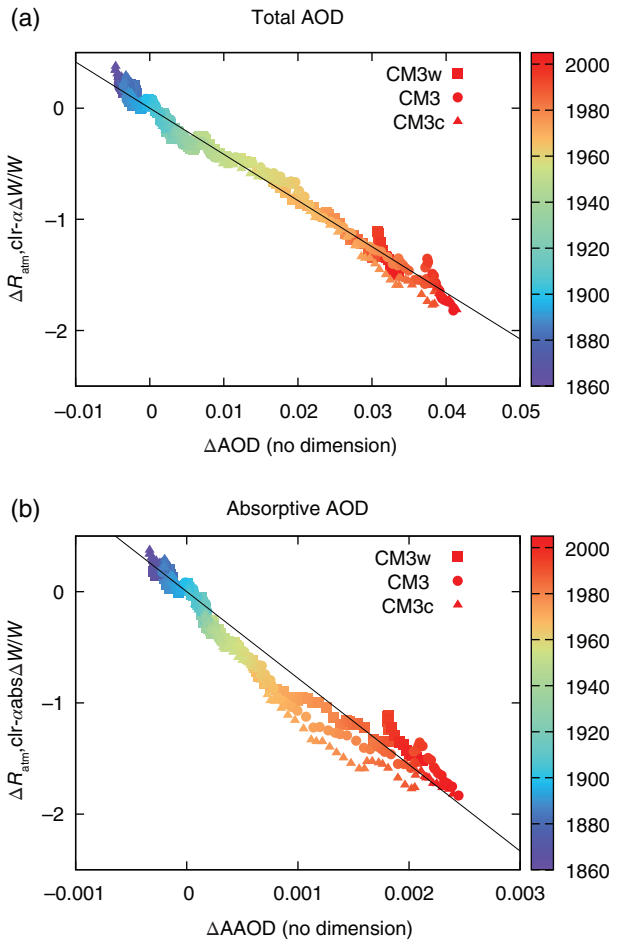

Figure 4. Scatter plot of the component in the clear-sky atmospheric radiative cooling that does not scale with changes to water vapor amount as a function of changes to global-mean (a) aerosol optical depth (AOD) and (b) absorptive AOD (AAOD). The black line shows a linear relationship (3) and (4) defined with (a) $\alpha = 0.26\,\mathrm{Wm^{-2}\%^{-1}}$ and $\beta = 41.5\,\mathrm{Wm^{-2}}$ and (b) $\alpha_{abs} = 0.265\,\mathrm{Wm^{-2}\%^{-1}}$ and $\beta_{abs} = 777.183\,\mathrm{Wm^{-2}}$ obtained as the inter-scenario averages shown in Tables 1 and 2.

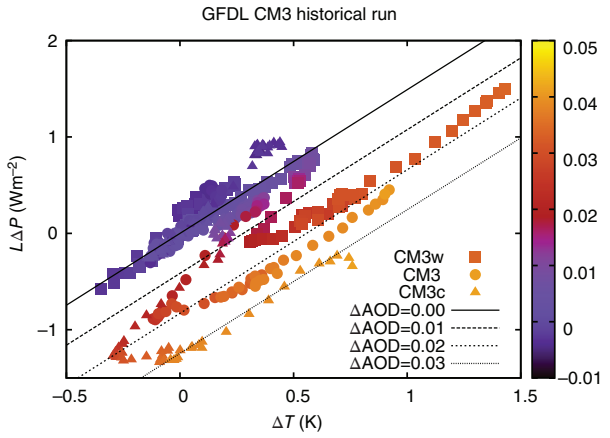

Figure 5. Scatter plot of the latent heating rate anomaly associated with global precipitation change as a function of the global-mean surface air temperature anomaly obtained from CM3w (square), CM3 (circle) and CM3c (triangle) scenario simulations colored according to the AOD anomaly (ΔAOD) labeled on the right. Linear relationships given by (7) are also shown for various specified values of ΔAOD as references.

threshold particle size, which causes less efficient precipitation as demonstrated by Suzuki *et al.* (2013) in the form of the microphysical statistics directly comparable to satellite observations. Given that the precipitation efficiency is a major factor that controls the aerosol scavenging, less efficient precipitation sets the condition for reduced aerosol scavenging, which could lead to larger aerosol loadings. This implies that differing assumptions of cloud microphysics modulate the aerosol scavenging process to induce different aerosol loadings, which in turn perturb global energy balance to result in significant changes to global precipitation.

4. Conclusion

This study performs analysis of the 20th century historical simulations by GFDL CM3 in an attempt to identify and quantify factors that determine the climatic change of global-mean precipitation. The well-known energy balance controls on global precipitation are reviewed to obtain a theoretical relationship describing the global precipitation change as a function of both changes to global-mean temperature and AOD in the context of historical climate change. This allows a quantification of contributions of aerosol radiative effects to global precipitation change in the whole picture of global energy balance. The theoretical relationships are applied to analyze the simulation data and demonstrate that the historical change of global precipitation is indeed decomposed into two parts, that is, a temperature-mediated component and an aerosol-dependent component. The former is further found to be dominated by the water vapor-induced clear-sky radiative cooling that is slightly modified by a small net negative cloud feedback on precipitation in the model analyzed. The latter quantifies contributions of the aerosol radiative effects to the energy balance controls on global precipitation change, which is proven significant at least in this particular climate model. This suggests that the aerosol direct radiative effect needs to be better constrained to improve predictions of global precipitation change. The magnitude of aerosol contribution to global precipitation is also found to vary among scenarios with alternate configurations of cloud microphysics that alter the precipitation efficiency, a major factor controlling the aerosol scavenging. The results imply how different assumptions of cloud microphysics could lead to different aerosol loadings that in turn perturb global energy balance to significantly change global precipitation. This proposes a possible coupling of aerosol–cloud interaction with aerosol–radiation interaction in the context of global energy balance.

Acknowledgements

Aspects of this study were supported by NOAA's Climate Program Office's Modeling, Analysis, Predictions, and Projections program with grant number NA15OAR4310153 and

JAXA/EarthCARE project. Part of the research was carried out at Jet Propulsion Laboratory, California Institute of Technology, under contract with NASA. Work at LLNL was performed under the auspices the U.S. Department of Energy by Lawrence Livermore National Laboratory under contract No. DE-AC52-07NA27344. The GFDL model data used for analysis is available from the corresponding author upon request. The authors declare no conflict of interest.

Supporting information

The following supporting information is available:

Figure S1. Time series of anomalies of (a) column water vapor, (b) Aerosol Optical Depth, (c) reflected shortwave radiation at TOA and (d) atmospheric radiative cooling obtained from the simulations.

Figure S2. Scatter plot of atmospheric cloud radiative effect as a function of global-mean surface air temperature colored according to simulation years.

References

Allen MR, Ingram WJ. 2002. Constraints on future changes in climate and the hydrologic cycle. *Nature* **419**: 224–232.

Andrews T, Forster PM, Boucher O, Bellouin N, Jones A. 2010. Precipitation, radiative forcing and global temperature change. *Geophysical Research Letters* **37**: L14701. https://doi.org/10.1029/2010GL043991.

DeAngelis AM, Qu X, Zelinka MD, Hall A. 2015. An observational radiative constraint on hydrologic cycle intensification. *Nature* **528**: 249–253. https://doi.org/10.1038/nature15770.

Donner LJ, Wyman BL, Hemler RS, Horowitz LW, Ming Y, Zhao M, Golaz J-C, Ginoux P, Lin S-J, Schwarzkopf MD, Austin J, Alaka G, Cooke WF, Delworth TL, Freidenreich SM, Gordon CT, Griffies SM, Held IM, Hurlin WJ, Klein SA, Knutson TR, Langenhorst AR, Lee H-C, Lin Y, Magi BI, Malyshev SL, Milly PCD, Naik V, Nath MJ, Pincus R, Ploshay JJ, Ramaswamy V, Seman CJ, Shevliakova E, Sirutis JJ, Stern WF, Stouffer RJ, Wilson RJ, Winton M, Wittenberg AT, Zeng F. 2011. The dynamical core, physical parameterizations, and basic simulation characteristics of the atmospheric component AM3 of the GFDL global coupled model CM3. *Journal of Climate* **24**: 3484–3519. https://doi.org/10.1175/2011JCLI3955.1.

Fläschner D, Mauritsen T, Stevens B. 2016. Understanding the intermodal spread in global-mean hydrological sensitivity. *Journal of Climate* **29**: 801–817. https://doi.org/10.1175/JCLI-D-15-0351.1.

Golaz J-C, Horowitz LW, Levy H. 2013. Cloud tuning in a coupled climate model: impact on 20th century warming. *Geophysical Research Letters* **40**: 2246–2251. https://doi.org/10.1002/grl.50232.

Golaz J-C, Salzmann M, Donner LJ, Horowitz LW, Ming Y, Zhao M. 2011. Sensitivity of the aerosol indirect effect to subgrid variability in the cloud parameterization of the GFDL Atmosphere General Circulation Model AM3. *Journal of Climate* **24**: 3145–3160. https://doi.org/10.1175/2010JCLI3945.1.

Mauritsen T, Stevens B. 2015. Missing iris effect as a possible cause of muted hydrological change and high climate sensitivity in models. *Nature Geoscience* **8**: 346–351.

Ming Y, Ramaswamy V, Persad G. 2010. Two opposing effects of absorbing aerosols on global-mean precipitation. *Geophysical Research Letters* **37**: L13701. https://doi.org/10.1029/2010GL042895.

Pendergrass AG, Hartmann DL. 2012. Global-mean precipitation and black carbon in AR4 simulations. *Geophysical Research Letters* **39**: L01703. https://doi.org/10.1029/2011GL050067.

Pendergrass AG, Hartmann DL. 2014. The atmospheric energy constraint on global-mean precipitation change. *Journal of Climate* **27**: 757–768. https://doi.org/10.1175/JCLI-D-13-00163.1.

Salzmann M. 2016. Global warming without global mean precipitation increase? *Science Advances* **2**: e1501572. https://doi.org/10.1126/sciadv.1501572.

Samset BH, Myhre G, Forster PM, Hodnebrog O, Andrews T, Faluvegi G, Flaschner D, Kasoar M, Kharin V, Kirkevag A, Lamarque J-F, Olivie D, Richardson T, Shindell D, Shine KP, Takemura T, Voulgarakis V. 2016. Fast and slow precipitation responses to individual climate forcers: a PDRMIP multimodel study. *Geophysiical Research Letters* **43**: 2782–2791. https://doi.org/10.1002/2016GL068064.

Stephens GL, Ellis T. 2008. Controls of global-mean precipitation increases in global warming GCM experiments. *Journal of Climate* **21**: 6141–6155. https://doi.org/10.1175/2008JCLI2144.1.

Stephens GL, Hu Y. 2010. Are climate-related changes to the character of global-mean precipitation predictable? *Environmental Research Letters* **5**: 025209. https://doi.org/10.1088/1748-9326/5/2/025209.

Suzuki K, Golaz J-C, Stephens GL. 2013. Evaluating cloud tuning in a climate model with satellite observations. *Geophysical Research Letters* **40**: 4464–4468. https://doi.org/10.1002/grl.50874.